Article

Molecular Cell

Misregulation of an Activity-Dependent Splicing Network as a Common Mechanism Underlying Autism Spectrum Disorders

Graphical Abstract

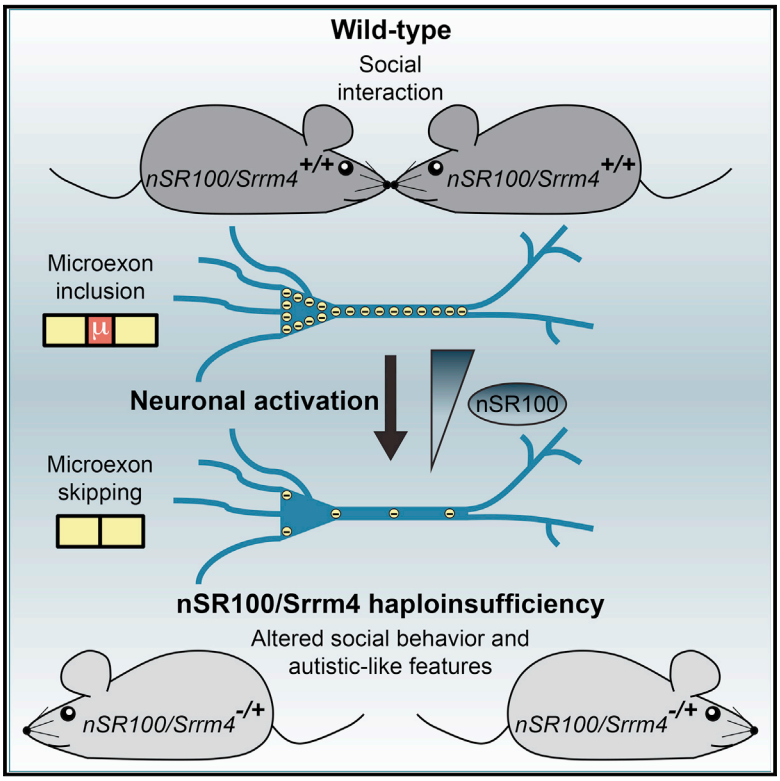

Authors

Mathieu Quesnel-Vallières, Zahra Dargaei, Manuel Irimia, ..., Melanie A. Woodin, Benjamin J. Blencowe, Sabine P. Cordes

Correspondence

b.blencowe@utoronto.ca (B.J.B.), cordes@lunenfeld.ca (S.P.C.)

In Brief

Quesnel-Vallières et al. report that mice haploinsufficient for the neuronal splicing regulator nSR100/SRRM4 display hallmark features of autism spectrum disorders. They further show that nSR100 is regulated by neuronal activity. These results causally implicate nSR100 as a molecular hub in ASD pathogenesis.

Highlights

- Multiple autistic-like features in nSR100/Srrm4 haploinsufficient mice
- nSR100 mutant mice have altered synaptic transmission and neuronal excitability
- Neuronal activation induces splicing changes observed in autistic individuals
- Neuronal activation alters splicing by reducing nSR100 levels

Accession Numbers

GSE89984

Quesnel-Vallières et al., 2016, Molecular Cell *64*, 1023–1034
December 15, 2016
http://dx.doi.org/10.1016/j.molcel.2016.11.033

Molecular Cell
Article

Misregulation of an Activity-Dependent Splicing Network as a Common Mechanism Underlying Autism Spectrum Disorders

Mathieu Quesnel-Vallières,[1,2,3] Zahra Dargaei,[4] Manuel Irimia,[5,6] Thomas Gonatopoulos-Pournatzis,[2] Joanna Y. Ip,[7] Mingkun Wu,[1,2] Timothy Sterne-Weiler,[2] Shinichi Nakagawa,[7] Melanie A. Woodin,[4] Benjamin J. Blencowe,[1,2,8,*] and Sabine P. Cordes[1,3,*]

[1]Department of Molecular Genetics, University of Toronto, Toronto, ON M5S 1A8, Canada
[2]Donnelly Centre, University of Toronto, Toronto, ON M5S 3E1, Canada
[3]Lunenfeld-Tanenbaum Research Institute, Mount Sinai Hospital, 600 University Avenue, Toronto, ON M5G 1X5, Canada
[4]Department of Cell and Systems Biology, University of Toronto, Toronto, ON M5S 3G5, Canada
[5]Centre for Genomic Regulation, Barcelona Institute of Science and Technology (BIST), Dr. Aiguader 88, Barcelona 08003, Spain
[6]Universitat Pompeu Fabra, Barcelona 08002, Spain
[7]RNA Biology Laboratory, RIKEN, Wako, Saitama 351-0198, Japan
[8]Lead Contact
*Correspondence: b.blencowe@utoronto.ca (B.J.B.), cordes@lunenfeld.ca (S.P.C.)
http://dx.doi.org/10.1016/j.molcel.2016.11.033

SUMMARY

A key challenge in understanding and ultimately treating autism is to identify common molecular mechanisms underlying this genetically heterogeneous disorder. Transcriptomic profiling of autistic brains has revealed correlated misregulation of the neuronal splicing regulator *nSR100/SRRM4* and its target microexon splicing program in more than one-third of analyzed individuals. To investigate whether nSR100 misregulation is causally linked to autism, we generated mutant mice with reduced levels of this protein and its target splicing program. Remarkably, these mice display multiple autistic-like features, including altered social behaviors, synaptic density, and signaling. Moreover, increased neuronal activity, which is often associated with autism, results in a rapid decrease in nSR100 and splicing of microexons that significantly overlap those misregulated in autistic brains. Collectively, our results provide evidence that misregulation of an nSR100-dependent splicing network controlled by changes in neuronal activity is causally linked to a substantial fraction of autism cases.

INTRODUCTION

Autism spectrum disorder (ASD) affects more than 1% of children and is highly heterogeneous with respect to its presentation and contributing genetic factors. All ASD patients exhibit deficits in socialization, which are often accompanied by environmental hypersensitivity. More than a thousand mutations and other forms of genetic variation affecting several hundred genes have been linked to ASD (Iossifov et al., 2014; Krumm et al., 2015; O'Roak et al., 2012). Some forms of ASD that accompany syndromic disorders, including fragile X syndrome (FXS), Rett (RTT) syndrome, and tuberous sclerosis complex (TSC), are caused by well-defined genetic alterations (de la Torre-Ubieta et al., 2016). However, most cases of ASD are idiopathic, i.e., they are of unknown or poorly defined genetic origin (Jeste and Geschwind, 2014). Because of the extensive heterogeneity associated with ASD, a key goal is to determine to what extent it is associated with the disruption of common molecular mechanisms and pathways (Mullins et al., 2016).

A common neurobiological feature of autism is a shift in the excitation/inhibition (E/I) ratio in synaptic formation and/or function, which affects neuronal network activity (Nelson and Valakh, 2015). Paradoxically, both increases and decreases in E/I ratios have been reported in murine models of ASD. For example, knockout of the gene encoding the eukaryotic translation initiation factor 4E-binding protein 2 (*Eif4ebp2*) results in increased translation of postsynaptic Neuroligin (Nlgn) proteins (Gkogkas et al., 2013), which in turn causes an increase in E/I ratios and autistic-like behaviors. Conversely, knockout of Nlgn3 (Tabuchi et al., 2007) or other synaptic proteins including Nrxn1 (Etherton et al., 2009) and Shank2 (Schmeisser et al., 2012) results in a reciprocal shift in the E/I balance toward inhibition, yet also causes autistic-like behaviors. It is also currently unclear whether such divergent activity levels associated with ASD involve alterations in common molecular mechanisms and pathways.

Transcriptome profiling employing microarrays and, more recently, high-throughput RNA sequencing (RNA-seq) of autistic brains has revealed common patterns of misregulated gene expression and alternative splicing (Chow et al., 2012; Gupta et al., 2014; Irimia et al., 2014; Voineagu et al., 2011). These altered transcriptomic profiles encompass modules of genes enriched in neuronal functions and with genetic links to ASD. These and a subsequent study also revealed misregulation of 5%–10% of alternative exons in patients with reduced levels of transcripts encoding members of the Rbfox family of RNA-binding splicing regulators (Voineagu et al., 2011; Weyn-Vanhentenryck et al., 2014).

Rbfox1 has been genetically linked to ASD in a small number of cases (Davis et al., 2012; Lee et al., 2016; Martin et al., 2007) and shown to regulate alternative splicing, mRNA stability, and translation of genes linked to brain development and ASD (Lee et al., 2016; Weyn-Vanhentenryck et al., 2014).

Recently, from comparisons of a larger cohort of autistic and control brain samples using a more sensitive RNA-seq analysis pipeline, it was observed that the splicing of 30%–40% of brain-specific microexons is disrupted in over one-third of analyzed idiopathic ASD individuals (Irimia et al., 2014). Microexons are a class of highly conserved, predominantly frame-preserving, and neuronal-enriched 3–27 nt cassette exons. They generally reside on protein surfaces, impact protein-protein interactions, and are significantly enriched in genes with critical roles in synaptic biology and with genetic links to ASD (Irimia et al., 2014; Li et al., 2015). Most neural microexons are controlled by nSR100, and *nSR100* mRNA levels are downregulated in autistic brains that display microexon skipping (Irimia et al., 2014). These observations have raised the intriguing possibility that disruption of nSR100 may represent a common mechanism underlying a substantial fraction of ASD cases. However, the mechanism(s) underlying reduced nSR100 expression and misregulation of its target splicing program in autistic brains have not been previously examined, nor has it been determined whether reduced expression of nSR100, or of any other splicing regulator, is causally linked to ASD.

ASD-associated cellular processes that control the formation and function of synapses, including transcription, translation, and post-translational modification, all respond to neuronal activity (Ebert and Greenberg, 2013). Likewise, alternative splicing and other forms of RNA processing and transport are dynamically regulated in response to changes in neuronal activity (Dictenberg et al., 2008; Eom et al., 2013; Iijima et al., 2011; Vuong et al., 2016; Xie and Black, 2001), and in some cases these changes have been linked to altered levels or activities of RNA-binding post-transcriptional regulators, including Rbfox1, Elav, and Sam68 (Gehman et al., 2011; Iijima et al., 2011; Ince-Dunn et al., 2012). However, the extent to which alternative splicing is regulated by changes in neuronal activity in the context of normal and disease/disorder-associated physiology has not been determined. Moreover, whether altered transcriptomic profiles encompassing reduced levels of nSR100 and its target microexon splicing program in autistic brains might be associated with changes in neuronal activity also has not been determined.

In this study, we employed heterozygous mutant mice expressing approximately 50% wild-type levels of nSR100 to assess whether reduced levels of this splicing regulator might be causally linked to ASD. Remarkably, these mice display several hallmark features of ASD, including altered social behavior and sensitivity to environmental stimuli, as well as altered synaptic transmission and neuronal excitability. Depolarization of wild-type neurons to induce increased neuronal activity, which can mimic changes observed in different models of ASD (Chahrour et al., 2012), and patient iPSC neurons (Acab and Muotri, 2015), resulted in widespread changes in the splicing of microexons controlled by nSR100 as well as those misregulated in patients with ASD. Consistent with these changes, nSR100 protein levels rapidly decrease upon stimulation of neuronal activity through a multifaceted mechanism that includes proteolytic degradation and a shift to expression of non-productive *nSR100* transcripts. Collectively, our data provide evidence that nSR100 constitutes a regulatory "hub" that is impacted by changes in neuronal activity that can arise in ASD, and that the disruption of this hub results in numerous ASD-like phenotypes.

RESULTS

nSR100 Haploinsufficiency Causes Autistic-like Neurodevelopmental and Behavioral Defects

To investigate whether reduced expression of nSR100 is causally linked to ASD-associated phenotypes, we analyzed mutant mice lacking one functional copy of the *nSR100/Srrm4* gene through a frameshifting deletion of exons 7 and 8 ($nSR100^{+/\Delta 7\text{-}8}$) (Quesnel-Vallières et al., 2015). These mice express ~50% of wild-type levels of protein (Figure 1A) and display intermediate levels of splicing of microexons and other target exons, relative to wild-type and homozygous mutant ($nSR100^{\Delta 7\text{-}8/\Delta 7\text{-}8}$) animals (Figures 1B and 1C). As such, they recapitulate misregulated patterns of splicing observed in autistic human brains (Irimia et al., 2014). $nSR100^{+/\Delta 7\text{-}8}$ mutant mice appear normal in tests for locomotion, habituation, short-term memory, olfaction, and hearing (Figure S1, available online), and they display either mild or no aberrant phenotypes in tests for responses to light stimuli and anxiety (Figure S2).

Individuals with ASD often have sensory gating defects that result in hypersensitivity to auditory stimuli (Baranek, 2002) and can display attenuated sensitivity to a pre-stimulus (i.e., prepulse) that normally desensitizes individuals to a subsequent startle response (Perry et al., 2007). Both male and female $nSR100^{+/\Delta 7\text{-}8}$ mice showed a significant increase in the amplitude of the startle response, and also a significant decrease in the pre-pulse inhibition of the startle response (Figure 2). These phenotypes may result from neuroanatomical defects associated with ASD that include altered cortical layering (Stoner et al., 2014), mis-wiring of brain circuitry (Rothwell et al., 2014; Willsey et al., 2013), and disturbance in the number of parvalbumin-expressing (Pv^+) fast-spiking interneurons (Cellot and Cherubini, 2013). Consistent with these possibilities, nSR100-deficient mice display aberrant cortical layering and axon guidance defects in the corpus callosum (Quesnel-Vallières et al., 2015), as well as an increase in the number of cortical Pv^+ interneurons (Figure S3). Thus, neurodevelopmental consequences of nSR100 reduction and/or loss are consistent with ASD-associated neurodevelopmental phenotypes.

Given that a unifying feature of ASD is its impact on socialization, we examined social behaviors in $nSR100^{+/\Delta 7\text{-}8}$ mice. Strikingly, when compared to wild-type mice in the three-chamber apparatus, a widely used test for social behaviors (Silverman et al., 2010), $nSR100^{+/\Delta 7\text{-}8}$ males significantly prefer interacting with an inanimate object over stranger mice (Figure 3A; $p = 0.015$, two-tailed t test). They are also strongly averse to social "novelty" when presented with stranger and familiar mice in the three-chamber apparatus (Figure 3B; $p = 0.018$, two-tailed t test). A decrease in social behavior

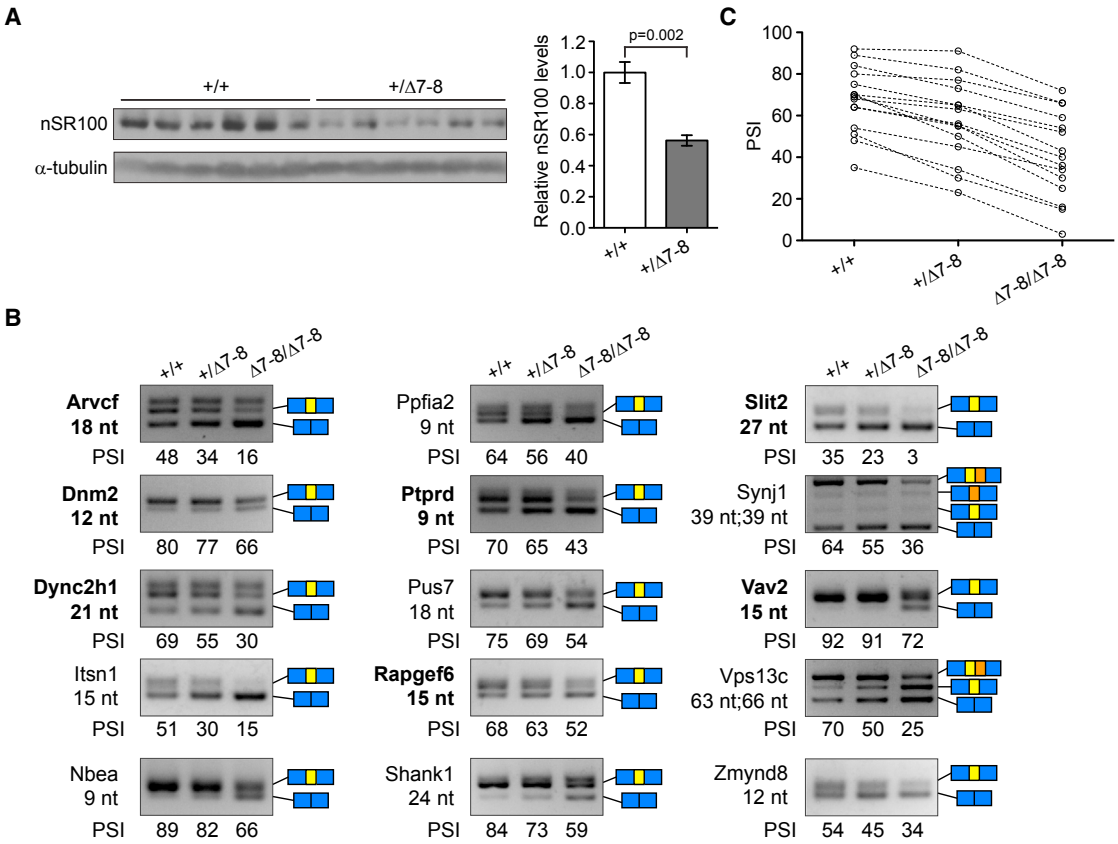

Figure 1. Intermediate Levels of nSR100 Protein and Alternative Splicing Defects in the Brain of *nSR100*$^{+/\Delta 7\text{-}8}$ Mutant Mice

(A) Immunoblotting was performed using an antibody to nSR100 on lysates from the cortex of six wild-type and six *nSR100*$^{+/\Delta 7\text{-}8}$ E18.5 embryos. Error bars, SEM.

(B) RT-PCR on nSR100 targets in wild-type, *nSR100*$^{+/\Delta 7\text{-}8}$, and *nSR100* $^{\Delta 7\text{-}8/\Delta 7\text{-}8}$ E18.5 cortex samples. The size of events surveyed is indicated below the gene names. Orthologous human microexons misregulated in ASD (Irimia et al., 2014) are highlighted in bold. Alternative exons, yellow or orange rectangles; constitutive exons, blue rectangles; PSI, percent spliced in.

(C) Scatterplot showing percent spliced in (PSI) of events presented in (B) with lines connecting the same event between different genotypes.

See also Figures S1 and S2.

was also observed in the reciprocal interaction test, where nSR100 mutant males spent significantly less time interacting than did wild-type mice (Figure 3C; p = 0.036, two-tailed t test). *nSR100*$^{+/\Delta 7\text{-}8}$ females also showed social behavior deficits, although these were not as pronounced as those observed for males in the three-chamber apparatus (Figure 3). ASD is almost five times more common in boys (1 in 42) than girls (1 in 189) (Christensen et al., 2016). It is remarkable that reduced levels of nSR100 result in hallmark social deficits in a manner reflecting the sexually dimorphic vulnerability to ASD seen in humans.

Altered Synaptic Transmission and Neuronal Excitability in *nSR100* Mutant Mice

Altered synaptic density and activity are additional phenotypes associated with ASD (Nelson and Valakh, 2015). Interestingly, microexons misregulated in nSR100-deficient mice and in autistic brains are enriched in genes involved in various aspects of synapse biology, including dynamics of neurotransmitter release (Irimia et al., 2014; Quesnel-Vallières et al., 2015). Moreover, primary cortical neurons from *nSR100*$^{\Delta 7\text{-}8/\Delta 7\text{-}8}$ mice harbor more glutamatergic (excitatory) and fewer GABAergic (inhibitory) synapses than wild-type neurons, as highlighted by immunofluorescence microscopy using antibodies specific for pre- and postsynaptic markers (Figure S4). Using mice specifically expressing enhanced green fluorescent protein (EGFP) in subsets of neurons (Thy1-EGFP reporter line), we also observe that the density of thin dendritic spines that lack the bulbous head characteristic of mature, functional spines is specifically increased in the somatosensory cortex of adult *nSR100*$^{+/\Delta 7\text{-}8}$ mice (Figure 4A). This defect in spine formation in *nSR100* mutant neurons suggests that synaptic activity might be affected in these neurons. Indeed, whole-cell recordings from adult *nSR100*$^{+/\Delta 7\text{-}8}$ cortical brain slices reveal a significant decrease in the frequency of both miniature and spontaneous excitatory postsynaptic currents (mEPSCs and sEPSCs; Figure 4B), suggesting a decrease in the frequency of glutamate release. No significant change in the amplitude of EPSCs was observed, indicating that reduced levels of nSR100 do not alter synaptic conductance. Similarly, in the case of inhibitory synaptic

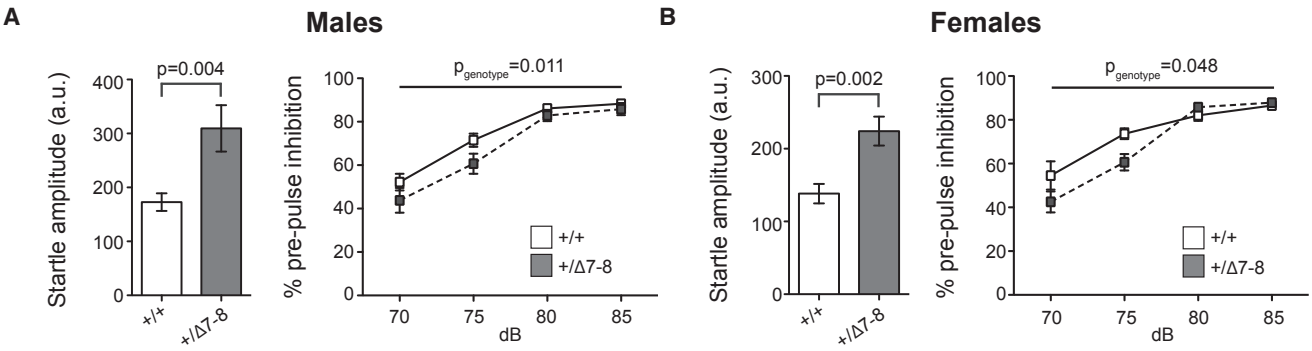

Figure 2. Sensory Hypersensitivity in *nSR100*$^{+/\Delta 7\text{-}8}$ Mice

The startle response is increased (D'Agostino-Pearson omnibus test followed by two-tailed t test) and the pre-pulse inhibition of the startle response is decreased in adult *nSR100*$^{+/\Delta 7\text{-}8}$ males (A) and females (B; two-way ANOVA, F(1,115) = 6.628 for males, F(1,143) = 3.962 for females). a.u., arbitrary units; dB, decibels. N = 13 males per genotype; N = 17 wild-type and 22 *nSR100*$^{+/\Delta 7\text{-}8}$ females.

See also Figure S3.

transmission, the frequency, but not amplitude, of miniature inhibitory postsynaptic currents (mIPSCs) is also decreased in adult *nSR100*$^{+/\Delta 7\text{-}8}$ cortical brain slices (Figure 4C). Our results thus support the conclusion that a decrease in nSR100 levels reduces synaptic transmission by disrupting the frequency of presynaptic neurotransmitter release.

In addition to synaptic transmission, neuronal circuit activity is also determined by intrinsic neuronal excitability. We found that *nSR100*$^{+/\Delta 7\text{-}8}$ neurons are less excitable than wild-type neurons (Figure 4D), despite having a similar resting membrane potential (Figure 4E). The increased number of glutamatergic synapses in culture, and the increased number of thin spines in vivo, may therefore represent a homeostatic attempt by neurons to normalize decreased synaptic transmission and excitability (Turrigiano, 2012). Collectively, our results demonstrate that reduced levels of nSR100 alter the density of excitatory and inhibitory synapses, and lead to an overall decrease in both excitatory and inhibitory synaptic transmission in the adult brain, both of which represent additional hallmark features of ASD.

Neuronal Activity Regulates a Large Program of Alternative Splicing

Neuronal activity has been shown to regulate alternative splicing (Iijima et al., 2011; Vuong et al., 2016; Xie, 2008; Xie and Black, 2001), and several activity-dependent pathways are associated with ASD (Ebert and Greenberg, 2013). These observations prompted us to systematically investigate whether nSR100 controls alternative splicing in response to neuronal activity. Accordingly, we used RNA-seq to detect all classes of alternative splicing events modulated by neuronal activity in cultured wild-type hippocampal neurons activated by depolarization with KCl treatment (Figure 5A; Tables S1 and S2). Remarkably, of 408 detected alternative microexons, 95 (23%) display altered splicing levels after 3 hr of KCl treatment, among which 88 (92%) display increased skipping and only 7 display higher inclusion levels (Figure 5B). Proportionately fewer (887/10,830; 8.1%) cassette exons >27 nt in length show changes in splicing levels during neuronal depolarization, and these are also preferentially skipped in activated neurons (747/887; 84.2%) (Figure 5B). RT-PCR assays confirmed splicing changes detected by RNA-seq for all 14 microexons tested (Figure S5A). Treating neurons with KCl for 6 hr did not significantly increase splicing changes (data not shown). Genes harboring activity-dependent alternative cassette exons (>27 nt) have functions primarily related to signal transduction and transcriptional regulation, whereas those with activity-dependent microexons relate primarily to vesicle transport (Figure 5C). Analysis of an independent RNA-seq dataset (Maze et al., 2015) from primary cortical mouse neurons treated with KCl for 5 hr gave comparable results (Figures S5B–S5D; Table S3). Our results thus demonstrate that an alternative splicing program comprising hundreds of events, including a significant fraction of neural microexons enriched in genes with synaptic functions, is dynamically regulated by neuronal activity.

Neuronal Activity-Dependent Microexons Are nSR100 Targets and Are Misregulated in Autism

Remarkably, 87.2% (75/86) of microexons displaying increased skipping in activated neurons are also more skipped upon loss of nSR100 in the mouse brain (Figure S6A; association p value = 3.7×10^{-13}, one-sided binomial test), and we additionally observe a significant overlap between microexons skipped upon neuronal activation and in autistic brains (Figure 6A; $p = 7.66 \times 10^{-5}$, ASD versus depolarization; $p = 3.78 \times 10^{-4}$, depolarization versus *nSR100* mutant; p = 0.039, ASD versus *nSR100* mutant; Fisher's exact test). Moreover, UGC motifs, which represent binding sites through which nSR100 promotes neural exon inclusion (Nakano et al., 2012; Raj et al., 2014), are significantly enriched immediately upstream of microexons, as well as of longer cassette exons that display increased skipping after neuronal activation (Figure 6B; $p = 3.95 \times 10^{-11}$ for microexons, $p = 1.22 \times 10^{-4}$ for longer cassette exons; two-tailed Mann-Whitney test). Taken together, these results suggest a direct and widespread role for nSR100 in the splicing of microexons that are dynamically involved in synaptic functions and that respond to external stimuli, and they further suggest that nSR100 is regulated by neuronal activity. Also of importance is that the results reveal that an altered splicing signature in the

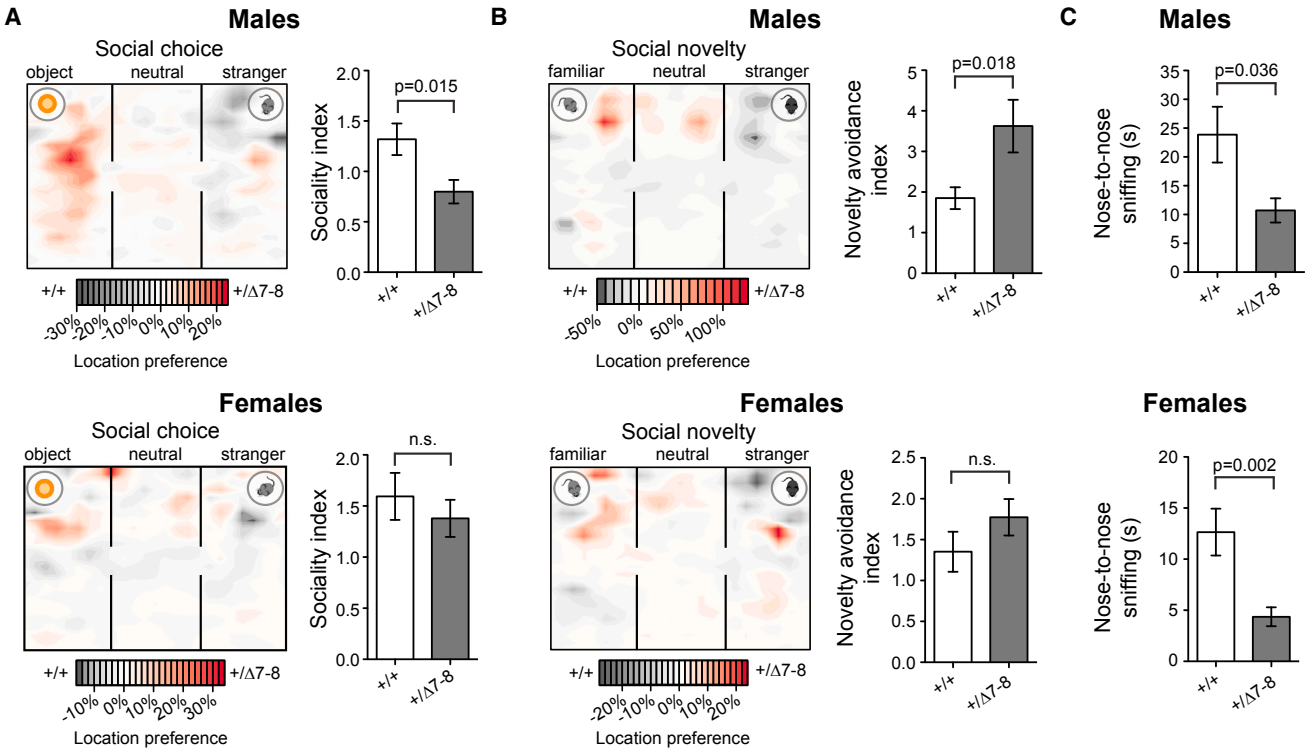

Figure 3. nSR100 Mutant Mice Display Autistic-like Behavior in a Sexually Dimorphic Manner

(A and B) Differential heatmaps showing where adult *nSR100*$^{+/\Delta 7\text{-}8}$ mice spent more time than wild-type mice (orange scale) and where wild-type mice spent more time than *nSR100*$^{+/\Delta 7\text{-}8}$ mice (gray scale) in the three-chamber social choice test (A) and in the social novelty test (B). Social behavior was measured as a sociality index in the social choice test (time interacting with stranger/time interacting with object) and as a social novelty avoidance index in the social novelty test (time spent in chamber with familiar mouse or in neutral chamber/time spent in chamber with stranger mouse). N = 17 wild-type and 15 *nSR100*$^{+/\Delta 7\text{-}8}$ males; N = 17 wild-type and 21 *nSR100*$^{+/\Delta 7\text{-}8}$ females.

(C) The reciprocal social interaction test was used to measure direct nose-to-nose interactions. N = 10 wild-type and 8 *nSR100*$^{+/\Delta 7\text{-}8}$ males; N = 6 wild-type and 10 *nSR100*$^{+/\Delta 7\text{-}8}$ females. D'Agostino-Pearson omnibus test followed by two-tailed t test. s, seconds. Error bars, SEM.

brains of ASD subjects is associated with increased neuronal activity.

To address the mechanism connecting these observations, we assayed nSR100 levels in response to depolarization. Remarkably, there is an ~2-fold decrease in nSR100 protein levels within 30 min after KCl treatment of primary neurons (Figure 6C). This decrease is reversible, as allowing 24 hr of recovery after 3 hr of KCl treatment restores nSR100 to pre-KCl treatment levels (Figure S6B). Moreover, this change is triggered by neuronal depolarization rather than osmotic effect since treating neurons with a concentration of NaCl osmotically equivalent to the 55 mM KCl treatment used above does not alter nSR100 protein levels (Figure S6C). The rapid decrease in nSR100 protein levels following depolarization suggests that it may be targeted by proteolysis. Treatment with the proteasomal inhibitor MG132 in the absence of depolarization results in a 2-fold increase in nSR100 protein levels, indicating that steady-state levels of nSR100 are regulated by proteasomal degradation (Figure 6D, lanes 1–3 versus lanes 4–6). Although maintaining MG132 treatment after the addition of KCl does not prevent a reduction in nSR100 levels following depolarization (Figure 6D, lanes 4–6 versus lanes 7–12), the increase in nSR100 levels observed during MG132 treatment is accompanied by a decrease in the magnitude of KCl-induced microexon skipping (Figure 6E).

To further assess whether the activity-dependent changes in microexon inclusion levels are a direct consequence of the reversible loss of nSR100 protein, we expressed nSR100 from a cDNA construct during KCl depolarization of Neuro2A cells. Importantly, increased expression of nSR100 during KCl treatment prevented the activity-dependent skipping of microexons (Figure S6D, lanes 1–6). Conversely, short hairpin RNA (shRNA) knockdown of nSR100 further reduced KCl-induced microexon inclusion changes (Figure S6D, lanes 7 and 8). Collectively, these and the results described above provide evidence that activity-dependent changes in microexon splicing are a direct consequence of reduced steady-state levels of nSR100, and that these changes occur through a proteasome-independent degradation pathway. Moreover, the results provide evidence that nSR100 function is likely neuronal activity dependent.

To further investigate possible additional mechanism(s) underlying reduced levels of nSR100, we analyzed activation-dependent changes in *nSR100* transcripts. *nSR100* transcripts harbor a 16 nt microexon and overlapping intron that display increased

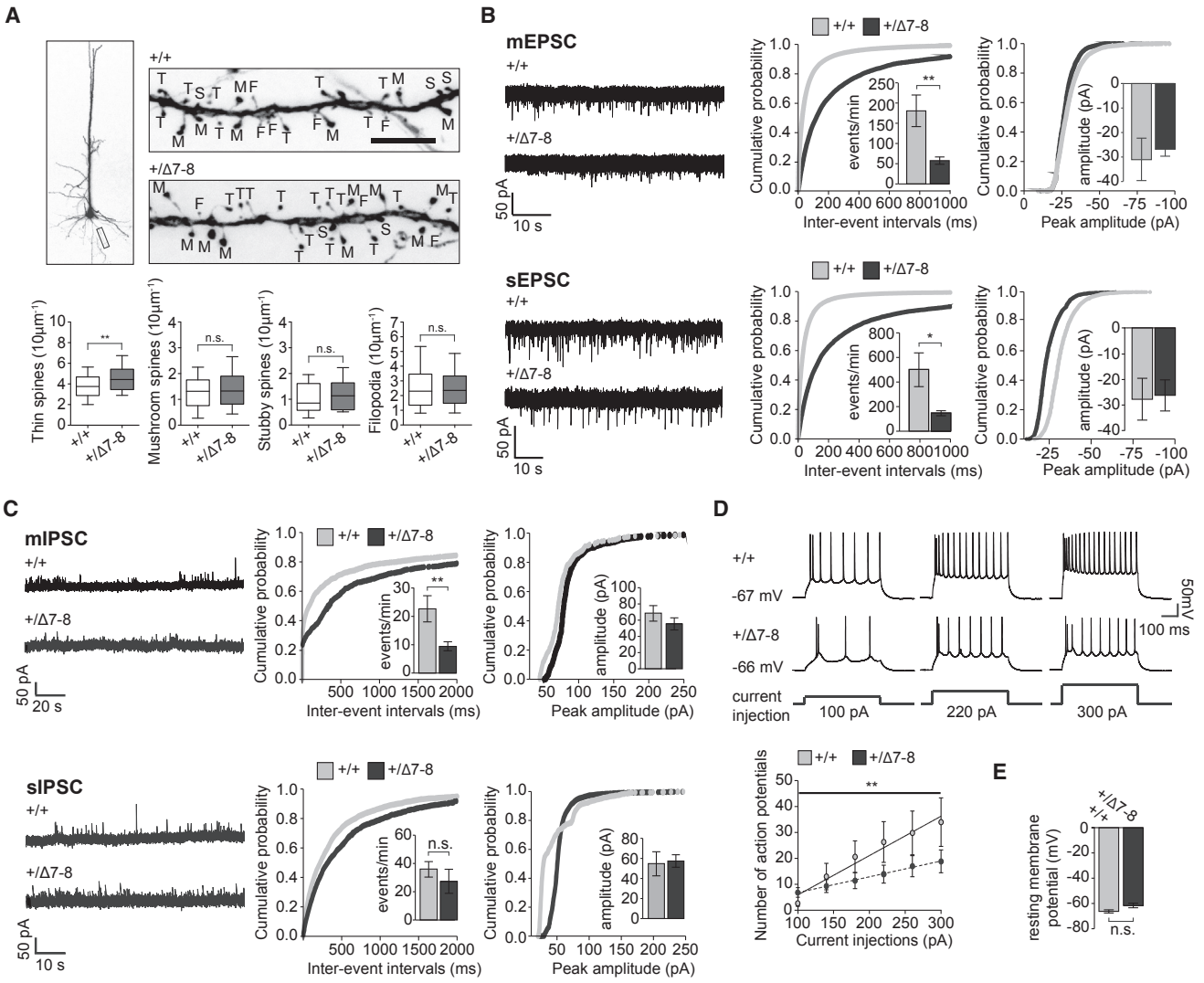

Figure 4. Impaired Synaptic Transmission and Excitability in *nSR100*$^{+/\Delta 7\text{-}8}$ Neurons

(A) The number and morphology of spines was characterized from EGFP^{+} pyramidal neurons of the somatosensory cortex from mice bearing the *Thy1-EGFP* transgene in a region of the dendritic arbor corresponding to the boxed area in the left panel. Spines were assessed as mushroom (M), thin (T), stubby (S), or filopodia (F). *nSR100*$^{+/\Delta 7\text{-}8}$ mice have a higher number of thin spines (**p = 0.006). N = 3 mice for each genotype, 21–27 dendrites per mouse. Two-tailed Mann-Whitney test; whiskers, 10th–90th percentiles. n.s., not significant.

(B) *nSR100*$^{+/\Delta 7\text{-}8}$ mice have a lower frequency but unaltered amplitude of mEPSCs and sEPSCs when compared to wild-type mice. Representative traces of mEPSCs or sEPSCs in wild-type and mutant neurons from the somatosensory cortex of adult mice are shown, and the frequency (center plots) and amplitude (right plots) of events were quantified. n = 5 cells per genotype. **p = 0.004 for mEPSC frequency and *p = 0.029 for sEPSC frequency, Mann-Whitney test. s, seconds; ms, milliseconds; pA, picoamperes.

(C) *nSR100*$^{+/\Delta 7\text{-}8}$ mice have a lower frequency but unaltered amplitude of mIPSCs, and unaltered sIPSCs when compared to wild-type mice. Representative traces of mIPSCs or sIPSCs in wild-type and mutant neurons from the somatosensory cortex of adult mice are shown, and the frequency (center plots) and amplitude (right plots) of events were quantified. n = 8 cells per genotype for sIPSCs; n = 8 cells per genotype for mIPSC frequency and n = 5 cells per genotype for mIPSC amplitude. **p = 0.002 for mIPSC frequency, Mann-Whitney. n.s., not significant.

(D) Evoked action potentials are less frequent in *nSR100*$^{+/\Delta 7\text{-}8}$ neurons. Representative traces are shown in the upper panel. The number of action potentials recorded when applying increasing steps of current injections for 500 ms were quantified (bottom panel). n = 6 wild-type and 14 *nSR100*$^{+/\Delta 7\text{-}8}$ cells. r^2 = 0.957 for wild-type and 0.996 for *nSR100*$^{+/\Delta 7\text{-}8}$, two-way ANOVA; F(1,108) = 8.776, **$p_{genotype}$ = 0.004. mV, millivolts.

(E) Resting potential of *nSR100*$^{+/\Delta 7\text{-}8}$ neurons does not significantly differ from wild-type neurons. n = 9 wild-type and 18 *nSR100*$^{+/\Delta 7\text{-}8}$ cells for resting potentials. Two-tailed t test.

All error bars are SEM. See also Figure S4.

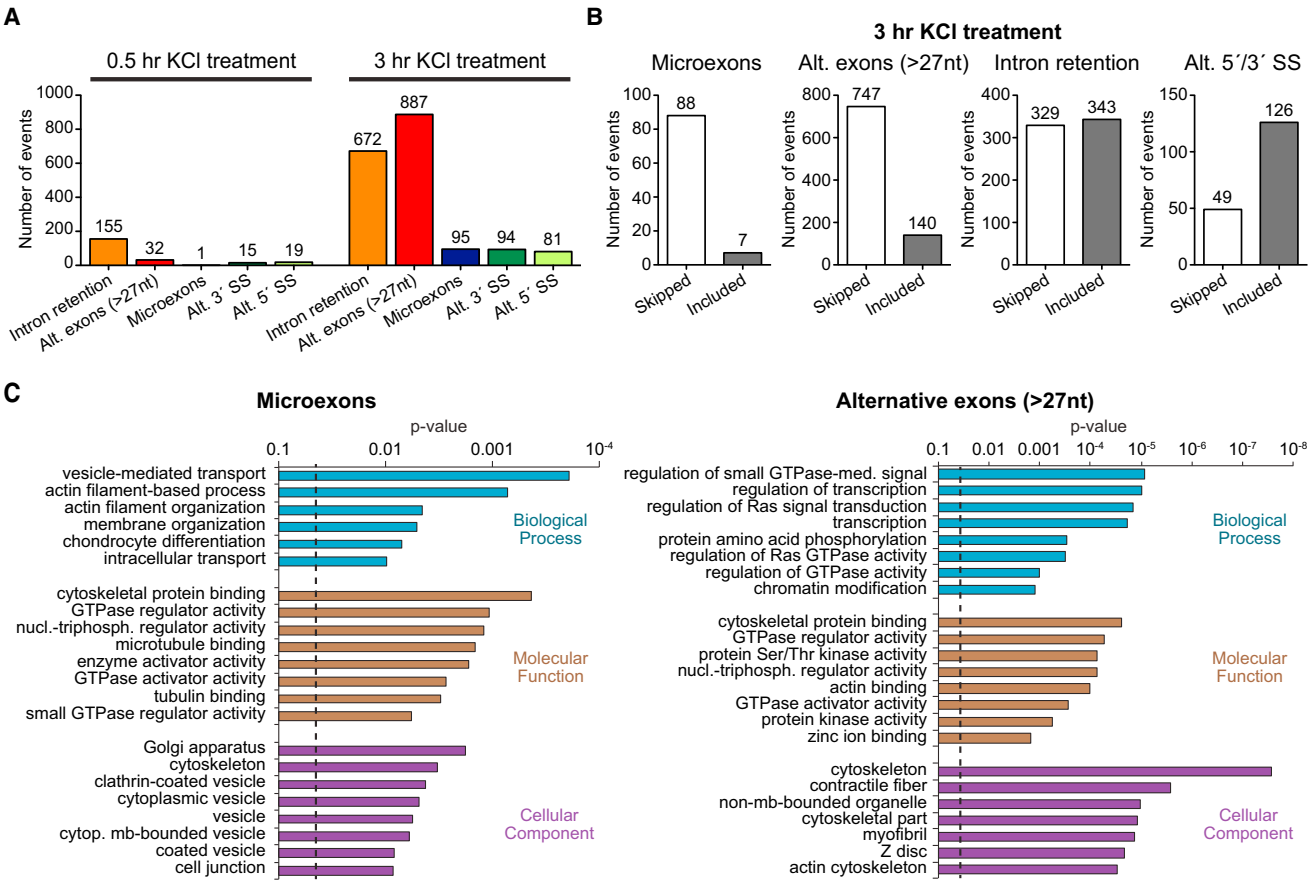

Figure 5. A Program of Neuronal Activity-Dependent Alternative Splicing

(A) Bar graphs depicting the number of alternative splicing events with percent spliced in (PSI), percent intron retention (PIR), or percent splice site usage (PSU) changes ≥15 after 0.5 and 3 hr of KCl treatment. The number of events included in each category is shown above the bars. Alt exons (>27 nt), alternative cassette exons longer than 27 nt; Alt. 5′ SS, alternative 5′ splice site; Alt. 3′ SS, alternative 3′ splice site.

(B) Microexons and cassette exons are preferentially skipped following neuronal activation, whereas retained introns show no directionality. The number of events included in each category is shown above the bars.

(C) Gene ontology enrichment analysis of genes containing microexons and cassette exons with |dPSI| ≥ 15 during neuronal activation.

See also Figure S5 and Tables S1, S2, S3, and S4.

inclusion and retention, respectively, upon neuronal activation (Figure 6F). Although the microexon is predicted to introduce a premature termination codon (PTC) with potential to elicit nonsense-mediated mRNA decay (NMD), steady-state levels of the microexon-containing spliced mRNAs and total nSR100 mRNAs increase slightly after 3 hr of activation (Figures 6F and 6G). Moreover, blocking NMD in Neuro2a cells with cycloheximide treatment did not affect the levels of any of the three *nSR100* isoforms assessed (Figure S6E). These alternative splicing events also do not appear to operate in a negative feedback regulatory loop, as overexpression of nSR100 in Neuro2A cells did not significantly affect the levels of inclusion of the microexon or retention of the intron (Figure S6F). However, in addition to increased splicing of the PTC-introducing microexon, we also observe an approximately 3-fold accumulation of *nSR100* transcripts containing the retained intron after 3 hr of KCl treatment (Figures 6F and 6G). To assess whether the increased levels of non-productive *nSR100* transcripts may contribute to reduced nSR100 protein levels following depolarization, we measured nSR100 protein half-life. Primary neurons were treated with cycloheximide and nSR100 levels were monitored over time by immunoblotting. These data reveal that the half-life of nSR100 is ~3 hr (Figure 6H). Given the ~2-fold decrease in nSR100 levels after 30 min of KCl depolarization (Figure 6C), it is therefore likely that the expression of non-productive *nSR100* transcripts contributes to reduced levels of nSR100 protein soon after depolarization. Taken together, our results indicate that neuronal activity-dependent skipping of microexons that are also misregulated in ASD occurs as a consequence of a multifaceted mechanism that includes the rapid proteolytic turnover of nSR100 and expression of non-productive *nSR100* transcripts.

DISCUSSION

In this study, we show that heterozygous mutant mice expressing reduced levels of nSR100 exhibit multiple key features of

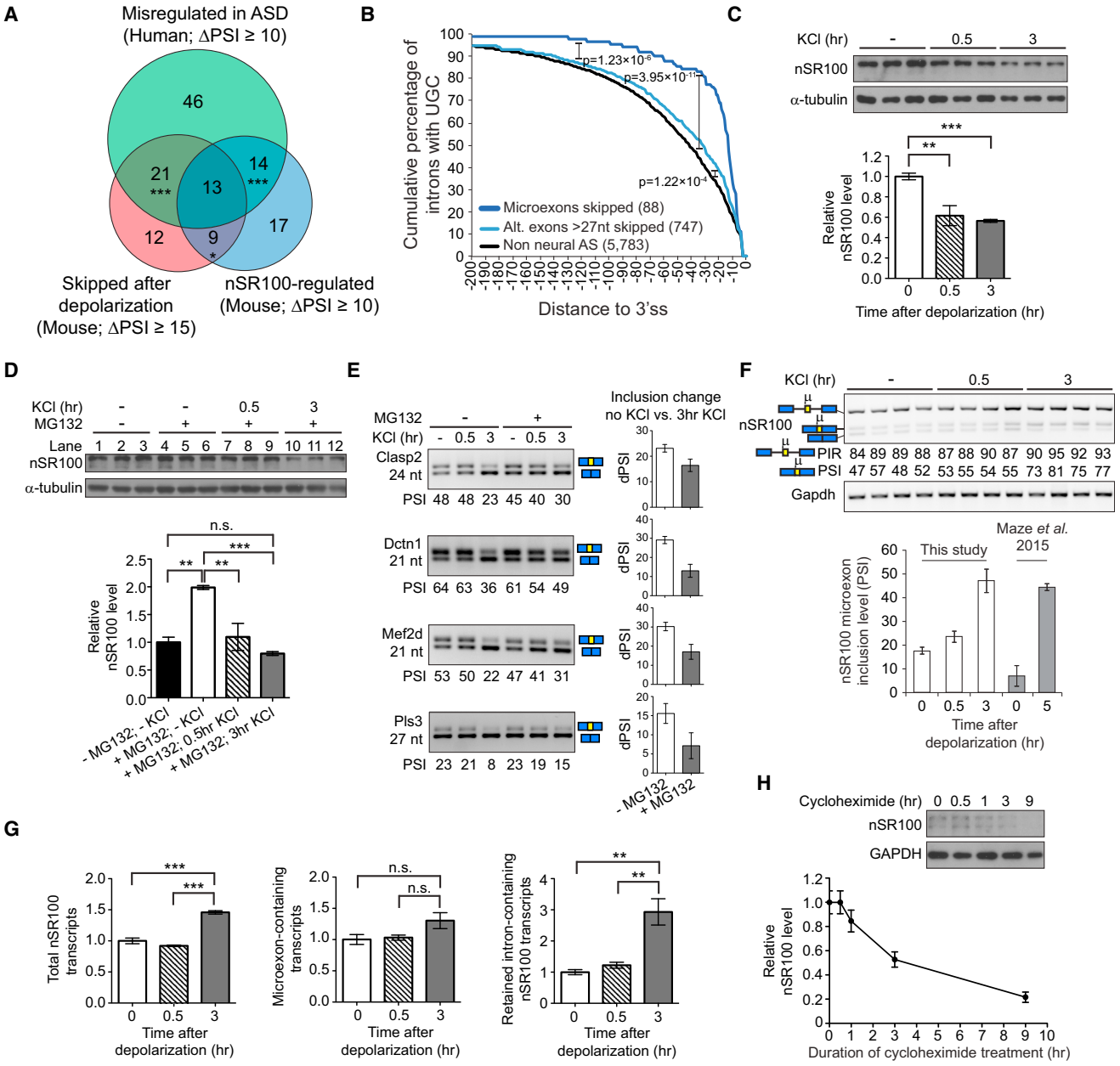

Figure 6. *nSR100*$^{+/\Delta 7\text{-}8}$ Neurons Mirror the Molecular Signature of KCl-Treated Neurons

(A) Venn diagram displaying the overlap between microexons that are skipped in humans with ASD (green) or upon neuronal activation (red), and nSR100-regulated microexons in mouse (blue). *p < 0.05; ***p < 0.0001.

(B) Cumulative distribution plots indicating the position of the first UGC motif within 200 nt upstream of neuronal activity-regulated microexons (dark blue) or longer cassette exons (light blue) versus non-neural alternative cassette exons (black). The number of exons used to analyze each subgroup is shown in parentheses.

(C) Quantification of nSR100 protein levels by immunoblotting of lysates from DIV11 cortical neurons treated with KCl.

(D) Quantification of nSR100 protein levels by immunoblotting of lysates from DIV11 cortical neurons treated with KCl in the presence or absence of proteasome inhibitor MG132.

(E) Comparison of microexon inclusion levels between DIV11 cortical neurons with or without MG132 treatment during KCl depolarization. RT-PCR was performed on RNA pooled from three biological replicates. dPSI between no and 3 hr KCl treatment is plotted in bar graphs. Error bars, SEM.

(F) Semi-quantitative RT-PCR (top panel) and RNA-seq (bottom panel) analyses of microexon splicing in *nSR100* transcripts after neuronal activation using DIV4 cortical neurons and DIV10 hippocampal neurons, respectively. An *nSR100* intron is also increasingly retained after activation. Percent intron retention (PIR) and PSI levels are indicated below the gel.

(legend continued on next page)

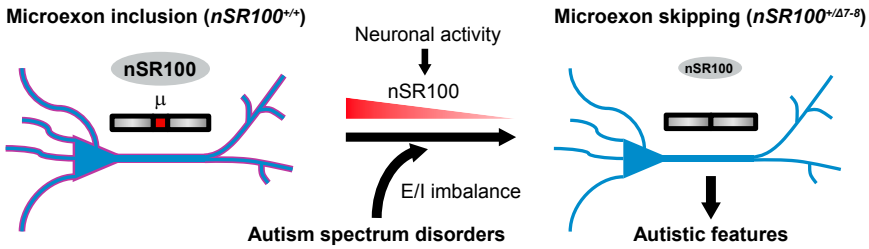

Figure 7. A Model for Activity-Dependent nSR100 Regulation and ASD

nSR100/Srrm4 expression activates the splicing of a program of microexons in healthy neurons. Experimental stimulation of neurons to mimic increased neuronal activity observed in some ASD models and patient iPSC neurons results in the rapid loss of expression of nSR100 protein and skipping of microexons (μ) that are also mis-regulated in autistic brains. Genetically reducing nSR100 levels reproduces the microexon splicing profile of activated wild-type neurons and autistic brains, and causes autistic-like behavior as well as other ASD-like phenotypes in mice.

ASD, including deficits in socialization that are most pronounced in male subjects, sensory hypersensitivity, and altered synaptic transmission and neuronal activity. Our results provide evidence for a causal role for disruption of an alternative splicing regulatory network in the development of autistic-like phenotypes, and further reveal a molecular mechanism linked to increased neuronal activity that likely underlies the disruption of this network in autistic human brains.

Our observation that the microexon splicing profiles of *nSR100* mutant neurons mirror those of activated primary neurons, and that nSR100 levels are reduced in response to neuronal activity, highlights a new mechanism that connects altered brain activity with ASD (Figure 7). Dynamic, activity-dependent modulation of nSR100 protein levels is likely important for normal neurodevelopment and function (Quesnel-Vallières et al., 2015), whereas, based on transcriptomic profiling of autistic brains (Irimia et al., 2014), it appears to represent a common target for disruption in ASD. These observations further suggest that neurological disorders linked to genetic alterations that impact neuronal activity may also disrupt this mechanism. For example, neuronal depolarization resulting from events such as stalled GABAergic neuron maturation or epileptic seizures, which accompany syndromic and some idiopathic ASD cases (Cellot and Cherubini, 2014; Spence and Schneider, 2009), could inappropriately reduce nSR100 levels and thereby cause or exacerbate neurodevelopmental or functional deficits associated with ASD.

The overall decrease in neuronal activity and synaptic signaling we observe in adult *nSR100*$^{+/\Delta 7\text{-}8}$ mice is presumably a direct consequence of reduced levels of nSR100 and the splicing of its target microexons (and possibly also of longer cassette exons) located in genes that are important for synaptic function. For example, reducing nSR100 levels may decrease the frequency of presynaptic neurotransmitter release by affecting the inclusion of microexons in genes governing vesicle-mediated transport and actin cytoskeleton and membrane reorganization (Figure 5C). The disruption of neurodevelopmental processes, including altered cortical neurogenesis and axon guidance (Quesnel-Vallières et al., 2015), or defective synaptic signaling during development (this study), while initially a direct consequence of disturbing nSR100-dependent splicing of neurodevelopmental genes, may also further contribute to the observed changes in the adult in a secondary manner (Rubenstein, 2010).

Given the activity-responsive nature of nSR100 and its splicing program, and that disruption of this splicing regulatory network is found in a substantial proportion of ASD cases, it is anticipated that future studies will further link nSR100 to ASD cases. In this regard, it is interesting to note that nSR100 controls a conserved microexon in *Eif4g* (Irimia et al., 2014). This factor binds eIF4e to form a translation initiation complex, and altered eIF4e activity has been linked to ASD (Gkogkas et al., 2013; Santini et al., 2013). nSR100 also regulates the splicing of microexons in additional activity-dependent genes such as the ASD-associated transcription factor *Mef2c*, as well as in synaptic genes with genetic links to ASD, including *Ank3*, *Nbea*, *Nrxn2*, and *Shank1* (this study and Bi et al., 2012; Castermans et al., 2003; Gauthier et al., 2011; Sato et al., 2012). Thus, multiple ASD-causing molecular pathways, including those that affect neuronal activity (de la Torre-Ubieta et al., 2016; Ebert and Greenberg, 2013; Mullins et al., 2016), likely converge on nSR100 and its target alternative splicing program. As such, nSR100 represents an attractive potential target for the development of new diagnostic and therapeutic approaches that may be applicable to a substantial proportion of ASD individuals.

EXPERIMENTAL PROCEDURES

Mice

All mice used in this study were C57BL/6. All experiments were conducted in compliance with the Animals for Research Act of Ontario and the Guidelines of the Canadian Council on Animal Care. The Centre for Phenogenomics (TCP) Animal Care Committee reviewed and approved all procedures conducted on animals at TCP.

Behavioral Tests

All behavioral tests were performed on wild-type and mutant mice generated from *nSR100*$^{+/\Delta 7\text{-}8}$ intercrosses and fostered by *nSR100*$^{+/\Delta 7\text{-}8}$ females. After weaning, mice were hosted in cages holding two to five siblings with a random distribution of genotypes. Behavior was either scored automatically with a tracking software or manually by an observer blind to the genotype of subject

(G) Quantification of total *nSR100* transcript levels and microexon-containing and retained intron-containing *nSR100* transcripts by qRT-PCR of KCl-treated DIV11 cortical neurons. Transcript levels were normalized to *Gapdh*, *Medd22*, and *Clptm1l*.

(H) Quantification of nSR100 protein levels in DIV4 cortical neurons treated with cycloheximide for 0.5, 1, 3, or 9 hr by immunoblotting.

See also Figure S6.

mice. Open-field, light-dark box, elevated zero maze, Y-maze, and olfaction tests as well as auditory brainstem response and electroretinography recordings were performed using standard protocols. In the three-chamber apparatus, subjects were given 10 min to interact with an object or a stranger mouse for the social choice test, immediately followed by an additional 10 min to interact with a familiar mouse or a new stranger mouse for the social novelty test. The reciprocal interaction test was performed after a period of at least 30 min of social isolation. Stranger mice were allowed to interact for 10 min in a clean cage. Measurements for the pre-pulse inhibition of the startle response were acquired following the International Mouse Phenotyping Resource of Standardized Screens protocol (https://www.mousephenotype.org/impress). See also Supplemental Experimental Procedures.

Dendritic Spines

A *Thy1-EGFP* mouse line (*Tg[Thy1-EGFP]MJrs /J#7788*) (Feng et al., 2000) was crossed with $nSR100^{+/\Delta 7\text{-}8}$ mice. Brains were harvested from 9- to 13-week-old wild-type or $nSR100^{+/\Delta 7\text{-}8}$ mice carrying only one copy of the *Thy1-EGFP* transgene. Dendrites from layer V-VI pyramidal neurons in the somatosensory cortex were imaged from 300 μm coronal slices. Spines were counted on dendritic segments of approximately 35 μm.

Primary Neuronal Cultures

For neuronal depolarization experiments, hippocampal neurons were prepared from embryonic day 16.5 (E16.5) embryos following a method described in Abe et al. (2004). Depolarization was induced by adding KCl at a final concentration of 55 mM and incubating for 0.5 or 3 hr. For all other experiments, cortical neurons were harvested from wild-type or $nSR100^{\Delta 7\text{-}8}$ mice at E18.5 and plated on glass coverslips coated with 2% Matrigel (Corning) for immunostaining experiments or on polystyrene coated with 2% Matrigel for RNA or protein extraction. RNA was extracted using Trizol following the manufacturer's instructions. Lysates were prepared in Tris lysis buffer. All experiments performed on neuronal cultures were performed in three or four biological replicates. See also Supplemental Experimental Procedures.

Electrophysiology

Cortical slices (300–400 μm) were prepared from 8- to 12-week-old mice in modified artificial cerebrospinal fluid (aCSF). Recordings were performed in whole-cell configuration on layer II/III pyramidal neurons in the somatosensory cortex. All recordings were performed on a minimum of three animals per genotype. See also Supplemental Experimental Procedures.

Computational Analysis

RNA-seq was performed on RNA extracted from days in vitro (DIV)10 hippocampal neurons from E16.5 embryos treated with 55 mM KCl in biological duplicates (see Table S4 for details on RNA-seq). We used *vast-tools* (Irimia et al., 2014) to detect and quantify alternative splicing from RNA-seq data. The threshold used to define neuronal activity-dependent alternative splicing events was as follows: alternative splicing events with sufficient read coverage (see Supplemental Experimental Procedures) that show a $\Delta PSI > 15$ between the two replicates for each time point and a minimum difference of 5 between ranges. Cumulative distribution of UGC motifs was performed as previously described (Raj et al., 2014). Gene ontology analysis was performed using DAVID (Huang et al., 2009) for GO_FAT categories. All multi-exonic genes with sufficient read coverage for at least one of their introns or exons (as defined by *vast-tools*) in our RNA-seq dataset were used as background. Alternative splicing inclusion levels for human orthologous microexons in autistic and control brains were obtained from Irimia et al. (2014) and data for $nSR100^{\Delta 7\text{-}8/\Delta 7\text{-}8}$ mice were obtained from Quesnel-Vallières et al. (2015). For the latter, we used microexons with sufficient read coverage in all four pairs of replicate experiments (wild-type and $nSR100^{\Delta 7\text{-}8/\Delta 7\text{-}8}$ RNA-seq) and with an average $|\Delta PSI| > 10$.

Immunoblotting

E18.5 brains were lysed in Tris lysis buffer (10 mM Tris, 150 mM NaCl, 1% NP-40, and 10% glycerol) and sonicated. Protein samples were immunoblotted with an anti-nSR100 polyclonal rabbit antibody (Calarco et al., 2009) diluted at 1:5,000 overnight at 4°C. Mouse anti-tubulin (T6074, Sigma) was used at 1:5,000 and incubated for 2–3 hr at room temperature. Horseradish peroxidase-conjugated anti-rabbit and anti-mouse antibodies were used at 1:5,000 and incubated for 1–2 hr at room temperature.

Immunofluorescence

Coronal sections (16 μm) from formaldehyde-fixed E18.5 embryonic or adult mouse brains were blocked and permeabilized in 5% BSA and 0.3% Triton X-100 in PBS with or without the M.O.M. kit (Vector Labs) for 1 hr at room temperature. All primary antibodies were incubated overnight at 4°C, with or without the M.O.M. kit. Antibodies were as follows: mouse anti-NeuN (mab377, Millipore) diluted to 1:200, rabbit anti-parvalbumin (PV27, Swant) diluted to 1:2,000, rabbit anti-vGlut1 (135 303, Synaptic Systems) diluted to 1:500, mouse anti-PSD-95 (ab2723, Abcam) diluted to 1:500, rabbit anti-vGAT (131 011, Synaptic Systems) diluted to 1:500, mouse anti-gephyrin (147 111, Synaptic Systems) diluted to 1:500, and chicken anti-MAP2 (ab5392, Abcam) diluted to 1:10,000. Secondary antibodies were goat anti-mouse, anti-rabbit, or anti-chicken coupled to Alexa 488, Alexa-568, Alexa-594, or Alexa-647 dyes (Abcam), all diluted to 1:500 and incubated for 1 hr at room temperature with or without the M.O.M. kit. Stained sections were mounted in Vectashield mounting medium with DAPI.

RT-PCR and qRT-PCR

Semi-quantitative RT-PCR was performed using the QIAGEN One-Step RT-PCR kit as per the manufacturer's instructions using 20 ng total RNA as template per 10 μL reaction and run on 2% or 4% agarose gels. Bands were quantified using Image Lab (BioRad) or ImageJ. Primer sequences are available upon request.

For qRT-PCR, RNA was converted into cDNA using the Maxima H Minus First Strand cDNA Synthesis kit (Thermo Scientific) as per the manufacturer's instructions. qRT-PCR was performed in technical triplicates using the SensiFAST SYBR No-ROX Kit (Bioline) and 2 ng cDNA per reaction.

Cellular Fractionation

Cellular fractionation was performed following the REAP method (Suzuki et al., 2010). Briefly, cells were harvested in PBS and resuspended in 0.1% NP-40 in PBS. After a brief spin, half of the supernatant was collected as the cytoplasmic fraction. The pellet was washed once in 0.1% NP-40 in PBS and then collected as the nuclear fraction. RNA was extracted using TRI Reagent (Sigma) as per the manufacturer's instructions.

ACCESSION NUMBERS

RNA-seq data have been deposited in the GEO database under ID code GEO: GSE89984. The unprocessed image files used to prepare the figures in this manuscript have been deposited to Mendeley Data and are available at http://dx.doi.org/10.17632/rmh678fmvs.1.

SUPPLEMENTAL INFORMATION

Supplemental Information includes Supplemental Experimental Procedures, six figures, and four tables and can be found with this article online at http://dx.doi.org/10.1016/j.molcel.2016.11.033.

AUTHOR CONTRIBUTIONS

Conceptualization, M.Q.-V., B.J.B., and S.P.C.; Methodology, M.Q.-V., Z.D., M.I., T.G.-P., J.Y.I., T.S.-W., M.W., S.N., M.A.W., B.J.B., and S.P.C.; Investigation, M.Q.-V., Z.D., M.I., T.G.-P., J.Y.I., and M.W.; Formal Analysis, M.Q.-V., Z.D., M.I., M.A.W., B.J.B., and S.P.C.; Writing – Original Draft, M.Q.-V., B.J.B., and S.P.C.; Writing – Review & Editing, M.Q.-V., Z.D., M.I., T.G.-P., J.Y.I., T.S.-W., S.N., M.A.W., B.J.B., and S.P.C.; Visualization, M.Q.-V., Z.D., M.I., T.G.-P., T.S.-W., M.A.W., B.J.B., and S.P.C.; Supervision, M.I., S.N., M.A.W., B.J.B., and S.P.C.; Project Administration, B.J.B. and S.P.C.

ACKNOWLEDGMENTS

Z.D. and M.I. contributed equally to this work. We thank N. Parikshak and D. Geschwind for generously sharing RNA-seq data from ASD patients; Z. Berberovic, L. Kelsey, and A. Leonelli for technical assistance on ABR, ERG, and mouse husbandry; and I. Vukobradovic, J. Georgiou, T. Lipina, and E. Ngoch for advice on behavioral tests. Members of the B.J.B. and S.P.C. laboratories are thanked for helpful discussions and critical review of the manuscript, and D. Torti, D. Leung, and G. O'Hanlon in the Donnelly Sequencing Centre are gratefully acknowledged for sequencing samples. This work was supported by CIHR grants to S.P.C. (MOP#111199 and MOP#142340), B.J.B. (MOP#14609 and FDN#148434), and M.A.W. (MOP#123466), and an ERC Starting Grant to M.I. (ERC-StG-LS2-637591). M.Q.V. was supported by CIHR and OGS scholarships. T.G.-P. was supported by EMBO and OIRM fellowships. B.J.B. holds the University of Toronto Banbury Chair in Medical Research.

Received: June 30, 2016
Revised: October 27, 2016
Accepted: November 22, 2016
Published: December 15, 2016

REFERENCES

Abe, K., Chisaka, O., Van Roy, F., and Takeichi, M. (2004). Stability of dendritic spines and synaptic contacts is controlled by alpha N-catenin. Nat. Neurosci. *7*, 357–363.

Acab, A., and Muotri, A.R. (2015). The use of induced pluripotent stem cell technology to advance autism research and treatment. Neurotherapeutics *12*, 534–545.

Baranek, G.T. (2002). Efficacy of sensory and motor interventions for children with autism. J. Autism Dev. Disord. *32*, 397–422.

Bi, C., Wu, J., Jiang, T., Liu, Q., Cai, W., Yu, P., Cai, T., Zhao, M., Jiang, Y.H., and Sun, Z.S. (2012). Mutations of ANK3 identified by exome sequencing are associated with autism susceptibility. Hum. Mutat. *33*, 1635–1638.

Calarco, J.A., Superina, S., O'Hanlon, D., Gabut, M., Raj, B., Pan, Q., Skalska, U., Clarke, L., Gelinas, D., van der Kooy, D., et al. (2009). Regulation of vertebrate nervous system alternative splicing and development by an SR-related protein. Cell *138*, 898–910.

Castermans, D., Wilquet, V., Parthoens, E., Huysmans, C., Steyaert, J., Swinnen, L., Fryns, J.P., Van de Ven, W., and Devriendt, K. (2003). The neurobeachin gene is disrupted by a translocation in a patient with idiopathic autism. J. Med. Genet. *40*, 352–356.

Cellot, G., and Cherubini, E. (2013). Functional role of ambient GABA in refining neuronal circuits early in postnatal development. Front. Neural Circuits *7*, 136.

Cellot, G., and Cherubini, E. (2014). GABAergic signaling as therapeutic target for autism spectrum disorders. Front Pediatr. *2*, 70.

Chahrour, M.H., Yu, T.W., Lim, E.T., Ataman, B., Coulter, M.E., Hill, R.S., Stevens, C.R., Schubert, C.R., Greenberg, M.E., Gabriel, S.B., and Walsh, C.A.; ARRA Autism Sequencing Collaboration (2012). Whole-exome sequencing and homozygosity analysis implicate depolarization-regulated neuronal genes in autism. PLoS Genet. *8*, e1002635.

Chow, M.L., Pramparo, T., Winn, M.E., Barnes, C.C., Li, H.R., Weiss, L., Fan, J.B., Murray, S., April, C., Belinson, H., et al. (2012). Age-dependent brain gene expression and copy number anomalies in autism suggest distinct pathological processes at young versus mature ages. PLoS Genet. *8*, e1002592.

Christensen, D.L., Baio, J., Van Naarden Braun, K., Bilder, D., Charles, J., Constantino, J.N., Daniels, J., Durkin, M.S., Fitzgerald, R.T., Kurzius-Spencer, M., et al.; Centers for Disease Control and Prevention (CDC) (2016). Prevalence and characteristics of autism spectrum disorder among children aged 8 years—autism and developmental disabilities monitoring network, 11 sites, United States, 2012. MMWR Surveill. Summ. *65*, 1–23.

Davis, L.K., Maltman, N., Mosconi, M.W., Macmillan, C., Schmitt, L., Moore, K., Francis, S.M., Jacob, S., Sweeney, J.A., and Cook, E.H. (2012). Rare inherited A2BP1 deletion in a proband with autism and developmental hemiparesis. Am. J. Med. Genet. A. *158A*, 1654–1661.

de la Torre-Ubieta, L., Won, H., Stein, J.L., and Geschwind, D.H. (2016). Advancing the understanding of autism disease mechanisms through genetics. Nat. Med. *22*, 345–361.

Dictenberg, J.B., Swanger, S.A., Antar, L.N., Singer, R.H., and Bassell, G.J. (2008). A direct role for FMRP in activity-dependent dendritic mRNA transport links filopodial-spine morphogenesis to fragile X syndrome. Dev. Cell *14*, 926–939.

Ebert, D.H., and Greenberg, M.E. (2013). Activity-dependent neuronal signalling and autism spectrum disorder. Nature *493*, 327–337.

Eom, T., Zhang, C., Wang, H., Lay, K., Fak, J., Noebels, J.L., and Darnell, R.B. (2013). NOVA-dependent regulation of cryptic NMD exons controls synaptic protein levels after seizure. eLife *2*, e00178.

Etherton, M.R., Blaiss, C.A., Powell, C.M., and Südhof, T.C. (2009). Mouse neurexin-1alpha deletion causes correlated electrophysiological and behavioral changes consistent with cognitive impairments. Proc. Natl. Acad. Sci. USA *106*, 17998–18003.

Feng, G., Mellor, R.H., Bernstein, M., Keller-Peck, C., Nguyen, Q.T., Wallace, M., Nerbonne, J.M., Lichtman, J.W., and Sanes, J.R. (2000). Imaging neuronal subsets in transgenic mice expressing multiple spectral variants of GFP. Neuron *28*, 41–51.

Gauthier, J., Siddiqui, T.J., Huashan, P., Yokomaku, D., Hamdan, F.F., Champagne, N., Lapointe, M., Spiegelman, D., Noreau, A., Lafrenière, R.G., et al. (2011). Truncating mutations in NRXN2 and NRXN1 in autism spectrum disorders and schizophrenia. Hum. Genet. *130*, 563–573.

Gehman, L.T., Stoilov, P., Maguire, J., Damianov, A., Lin, C.H., Shiue, L., Ares, M., Jr., Mody, I., and Black, D.L. (2011). The splicing regulator Rbfox1 (A2BP1) controls neuronal excitation in the mammalian brain. Nat. Genet. *43*, 706–711.

Gkogkas, C.G., Khoutorsky, A., Ran, I., Rampakakis, E., Nevarko, T., Weatherill, D.B., Vasuta, C., Yee, S., Truitt, M., Dallaire, P., et al. (2013). Autism-related deficits via dysregulated eIF4E-dependent translational control. Nature *493*, 371–377.

Gupta, S., Ellis, S.E., Ashar, F.N., Moes, A., Bader, J.S., Zhan, J., West, A.B., and Arking, D.E. (2014). Transcriptome analysis reveals dysregulation of innate immune response genes and neuronal activity-dependent genes in autism. Nat. Commun. *5*, 5748.

Huang, W., Sherman, B.T., and Lempicki, R.A. (2009). Systematic and integrative analysis of large gene lists using DAVID bioinformatics resources. Nat. Protoc. *4*, 44–57.

Iijima, T., Wu, K., Witte, H., Hanno-Iijima, Y., Glatter, T., Richard, S., and Scheiffele, P. (2011). SAM68 regulates neuronal activity-dependent alternative splicing of neurexin-1. Cell *147*, 1601–1614.

Ince-Dunn, G., Okano, H.J., Jensen, K.B., Park, W.Y., Zhong, R., Ule, J., Mele, A., Fak, J.J., Yang, C., Zhang, C., et al. (2012). Neuronal Elav-like (Hu) proteins regulate RNA splicing and abundance to control glutamate levels and neuronal excitability. Neuron *75*, 1067–1080.

Iossifov, I., O'Roak, B.J., Sanders, S.J., Ronemus, M., Krumm, N., Levy, D., Stessman, H.A., Witherspoon, K.T., Vives, L., Patterson, K.E., et al. (2014). The contribution of de novo coding mutations to autism spectrum disorder. Nature *515*, 216–221.

Irimia, M., Weatheritt, R.J., Ellis, J.D., Parikshak, N.N., Gonatopoulos-Pournatzis, T., Babor, M., Quesnel-Vallières, M., Tapial, J., Raj, B., O'Hanlon, D., et al. (2014). A highly conserved program of neuronal microexons is misregulated in autistic brains. Cell *159*, 1511–1523.

Jeste, S.S., and Geschwind, D.H. (2014). Disentangling the heterogeneity of autism spectrum disorder through genetic findings. Nat. Rev. Neurol. *10*, 74–81.

Krumm, N., Turner, T.N., Baker, C., Vives, L., Mohajeri, K., Witherspoon, K., Raja, A., Coe, B.P., Stessman, H.A., He, Z.X., et al. (2015). Excess of rare, inherited truncating mutations in autism. Nat. Genet. *47*, 582–588.

Lee, J.A., Damianov, A., Lin, C.H., Fontes, M., Parikshak, N.N., Anderson, E.S., Geschwind, D.H., Black, D.L., and Martin, K.C. (2016). Cytoplasmic Rbfox1

regulates the expression of synaptic and autism-related genes. Neuron *89*, 113–128.

Li, Y.I., Sanchez-Pulido, L., Haerty, W., and Ponting, C.P. (2015). RBFOX and PTBP1 proteins regulate the alternative splicing of micro-exons in human brain transcripts. Genome Res. *25*, 1–13.

Martin, C.L., Duvall, J.A., Ilkin, Y., Simon, J.S., Arreaza, M.G., Wilkes, K., Alvarez-Retuerto, A., Whichello, A., Powell, C.M., Rao, K., et al. (2007). Cytogenetic and molecular characterization of A2BP1/FOX1 as a candidate gene for autism. Am. J. Med. Genet. B. Neuropsychiatr. Genet. *144B*, 869–876.

Maze, I., Wenderski, W., Noh, K.M., Bagot, R.C., Tzavaras, N., Purushothaman, I., Elsässer, S.J., Guo, Y., Ionete, C., Hurd, Y.L., et al. (2015). Critical role of histone turnover in neuronal transcription and plasticity. Neuron *87*, 77–94.

Mullins, C., Fishell, G., and Tsien, R.W. (2016). Unifying views of autism spectrum disorders: a consideration of autoregulatory feedback loops. Neuron *89*, 1131–1156.

Nakano, Y., Jahan, I., Bonde, G., Sun, X., Hildebrand, M.S., Engelhardt, J.F., Smith, R.J., Cornell, R.A., Fritzsch, B., and Bánfi, B. (2012). A mutation in the Srrm4 gene causes alternative splicing defects and deafness in the Bronx waltzer mouse. PLoS Genet. *8*, e1002966.

Nelson, S.B., and Valakh, V. (2015). Excitatory/inhibitory balance and circuit homeostasis in autism spectrum disorders. Neuron *87*, 684–698.

O'Roak, B.J., Vives, L., Girirajan, S., Karakoc, E., Krumm, N., Coe, B.P., Levy, R., Ko, A., Lee, C., Smith, J.D., et al. (2012). Sporadic autism exomes reveal a highly interconnected protein network of de novo mutations. Nature *485*, 246–250.

Perry, W., Minassian, A., Lopez, B., Maron, L., and Lincoln, A. (2007). Sensorimotor gating deficits in adults with autism. Biol. Psychiatry *61*, 482–486.

Quesnel-Vallières, M., Irimia, M., Cordes, S.P., and Blencowe, B.J. (2015). Essential roles for the splicing regulator nSR100/SRRM4 during nervous system development. Genes Dev. *29*, 746–759.

Raj, B., Irimia, M., Braunschweig, U., Sterne-Weiler, T., O'Hanlon, D., Lin, Z.Y., Chen, G.I., Easton, L.E., Ule, J., Gingras, A.C., et al. (2014). A global regulatory mechanism for activating an exon network required for neurogenesis. Mol. Cell *56*, 90–103.

Rothwell, P.E., Fuccillo, M.V., Maxeiner, S., Hayton, S.J., Gokce, O., Lim, B.K., Fowler, S.C., Malenka, R.C., and Südhof, T.C. (2014). Autism-associated neuroligin-3 mutations commonly impair striatal circuits to boost repetitive behaviors. Cell *158*, 198–212.

Rubenstein, J.L. (2010). Three hypotheses for developmental defects that may underlie some forms of autism spectrum disorder. Curr. Opin. Neurol. *23*, 118–123.

Santini, E., Huynh, T.N., MacAskill, A.F., Carter, A.G., Pierre, P., Ruggero, D., Kaphzan, H., and Klann, E. (2013). Exaggerated translation causes synaptic and behavioural aberrations associated with autism. Nature *493*, 411–415.

Sato, D., Lionel, A.C., Leblond, C.S., Prasad, A., Pinto, D., Walker, S., O'Connor, I., Russell, C., Drmic, I.E., Hamdan, F.F., et al. (2012). SHANK1 deletions in males with autism spectrum disorder. Am. J. Hum. Genet. *90*, 879–887.

Schmeisser, M.J., Ey, E., Wegener, S., Bockmann, J., Stempel, A.V., Kuebler, A., Janssen, A.L., Udvardi, P.T., Shiban, E., Spilker, C., et al. (2012). Autistic-like behaviours and hyperactivity in mice lacking ProSAP1/Shank2. Nature *486*, 256–260.

Silverman, J.L., Yang, M., Lord, C., and Crawley, J.N. (2010). Behavioural phenotyping assays for mouse models of autism. Nat. Rev. Neurosci. *11*, 490–502.

Spence, S.J., and Schneider, M.T. (2009). The role of epilepsy and epileptiform EEGs in autism spectrum disorders. Pediatr. Res. *65*, 599–606.

Stoner, R., Chow, M.L., Boyle, M.P., Sunkin, S.M., Mouton, P.R., Roy, S., Wynshaw-Boris, A., Colamarino, S.A., Lein, E.S., and Courchesne, E. (2014). Patches of disorganization in the neocortex of children with autism. N. Engl. J. Med. *370*, 1209–1219.

Suzuki, K., Bose, P., Leong-Quong, R.Y., Fujita, D.J., and Riabowol, K. (2010). REAP: A two minute cell fractionation method. BMC Res. Notes *3*, 294.

Tabuchi, K., Blundell, J., Etherton, M.R., Hammer, R.E., Liu, X., Powell, C.M., and Südhof, T.C. (2007). A neuroligin-3 mutation implicated in autism increases inhibitory synaptic transmission in mice. Science *318*, 71–76.

Turrigiano, G. (2012). Homeostatic synaptic plasticity: local and global mechanisms for stabilizing neuronal function. Cold Spring Harb. Perspect. Biol. *4*, a005736.

Voineagu, I., Wang, X., Johnston, P., Lowe, J.K., Tian, Y., Horvath, S., Mill, J., Cantor, R.M., Blencowe, B.J., and Geschwind, D.H. (2011). Transcriptomic analysis of autistic brain reveals convergent molecular pathology. Nature *474*, 380–384.

Vuong, C.K., Black, D.L., and Zheng, S. (2016). The neurogenetics of alternative splicing. Nat. Rev. Neurosci. *17*, 265–281.

Weyn-Vanhentenryck, S.M., Mele, A., Yan, Q., Sun, S., Farny, N., Zhang, Z., Xue, C., Herre, M., Silver, P.A., Zhang, M.Q., et al. (2014). HITS-CLIP and integrative modeling define the Rbfox splicing-regulatory network linked to brain development and autism. Cell Rep. *6*, 1139–1152.

Willsey, A.J., Sanders, S.J., Li, M., Dong, S., Tebbenkamp, A.T., Muhle, R.A., Reilly, S.K., Lin, L., Fertuzinhos, S., Miller, J.A., et al. (2013). Coexpression networks implicate human midfetal deep cortical projection neurons in the pathogenesis of autism. Cell *155*, 997–1007.

Xie, J. (2008). Control of alternative pre-mRNA splicing by Ca(++) signals. Biochim. Biophys. Acta *1779*, 438–452.

Xie, J., and Black, D.L. (2001). A CaMK IV responsive RNA element mediates depolarization-induced alternative splicing of ion channels. Nature *410*, 936–939.